Pure & Appl. Chem., Vol. 63, No. 10, pp. 1503–1510, 1991.
Printed in Great Britain.

Phase transitions arising from intramolecular electron-transfer in mixed-valence complexes *

Michio Sorai‡ and David N. Hendrickson¶

‡ Microcalorimetry Research Center, Faculty of Science, Osaka university, Toyonaka, Osaka 560, Japan

¶ Department of Chemistry, University of California at San Diego, La Jolla, California 92093-0506, U.S.A.

Abstract Many of the oxo-centered trinuclear transition-metal acetate complexes with the formula $[M(III)_2M(II)O(O_2CCH_3)_6L_3]S$ (**M**: Fe or Mn, L: monodentate ligand, **S**: solvate molecule) have been shown to convert from a statically valence-trapped state at low temperatures to valence-detrapped states at high temperatures, in which the mixed-valence complex is dynamically interconverting between three or four configurations corresponding to the minima on the ground-state adiabatic potential-energy surface. Our recent heat-capacity measurements have clearly demonstrated that the intramolecular electron-transfer event in these complexes occurs as phase transitions in cooperation with orientational disordering of the **S** that is not explicitly coordinated to the central metal ions **M**. Although, depending on **S**, the transition entropy is widely altered from complex to complex, mechanisms of the phase transitions can be interpreted in terms of intermolecular interactions between the distortion dipole of the complex and the permanent dipole of the solvate molecule **S**. The present paper reviews thermal properties of seven complexes having different combinations of **M**, L, and **S**. Particularly emphasized is the importance of complementary roles between the macroscopic entropic aspects and the microscopic aspects derived from spectroscopic and structural studies.

INTRODUCTION

Phase transitions often encountered in the solid state play a diagnostic role to elucidate what kind of intermolecular interactions stabilizes the crystal lattice of a given system. Phase transitions hitherto well-known are the order-disorder type and the displacive type. The former involves a change in the orientational alignment of molecular- or spin-axes, while the latter concerns the displacement of atomic- or molecular-positions. Since the intramolecular electronic energy is much greater than the intermolecular potential energy, the molecular structure remains unchanged before and after a phase transition for these systems; a change in the electronic energy of a molecule is sufficiently small to be neglected. Recently, however, new types of phase transitions have drawn many scientists' attention. Here electrons are directly concerned and a change in the electronic state is strongly coupled with a change in the lattice. These transitions involve the spin-crossover phenomena occurring between high- and low-spin states, the intramolecular electron-transfer in mixed-valence complexes, the metal-nonmetal transition known as the Peierls transition, the thermochromic phenomena, the neutral-ionic transition due to charge-transfer mechanism and so on.

Of these, the mixed-valence problem (refs 1-3) seems to be of particular interest in that the mechanisms of intramolecular electron-transfer in the solid state may give a broad clue to redox reactions and even electron-transfers in biological systems. The mixed-valence compounds intensively studied are the oxo-centered, basic iron acetates with general composition $[Fe(III)_2Fe(II)O(O_2CCH_3)_6(base)_3]\cdot$(solvate) and biferrocenium salts. Many of these complexes have been shown to convert from being valence-trapped at low temperatures to valence-

* Contribution No. 25 from the Microcalorimetry Research Center.

detrapped at high temperatures. One of the remarkable discoveries at the initial stage of these investigations was that the solvate molecules and the anions not explicitly coordinated to the central metal ions have a dramatic effect on the electron-transfer rate. For example, variable-temperature ^{57}Fe Mössbauer spectra of $[Fe_3O(O_2CCH_3)_6(py)_3](py)$, where py is pyridine, clearly show the onset of valence-detrapping at ~117 K, while the nonsolvate analogue $[Fe_3O(O_2CCH_3)_6(py)_3]$ remains in the valence-trapped state even at 315 K (ref. 4). This fact implies that the solvate molecules play a crucial role in the intramolecular electron-transfer event. In order to clarify the mechanisms of coupling between these moieties and the intramolecular electron-transfer, various spectroscopic and structural studies have been performed. We are trying to approach the mixed-valence phenomena from a thermodynamic standpoint and reported the first result of heat-capacity measurements of the mixed-valence complex $[Fe_3O(O_2CCH_3)_6(py)_3](py)$ in 1985 (ref. 5). Thermodynamic studies, in particular heat capacity measurements, serve as a powerful tool to elucidate energetic and entropic aspects of a phenomenon, from which one can obtain conclusive evidence as to whether or not a phase transition exists. Moreover, based on the transition entropy, it is possible to count up all candidates for the degrees of freedom excited when a phase transition occurs. The present paper describes calorimetric studies of a series of the mixed-valence trinuclear complexes, and emphasizes complementary roles between the macroscopic entropic aspects and the microscopic aspects derived from spectroscopic and structural studies.

INTRAMOLECULAR ELECTRON-TRANSFER IN THE TRINUCLEAR MIXED-VALENCE COMPLEXES

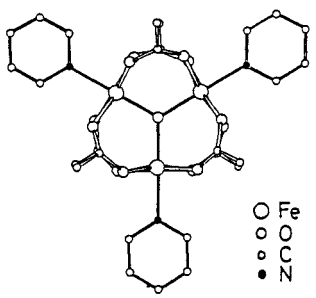

Fig. 1. Molecular structure of the trinuclear mixed-valence complex.

Oxo-centered, trinuclear transition-metal acetate complexes with the formula $[M(III)_2M(II)O(O_2CCH_3)_6L_3]\cdot S$ form a well-studied category of mixed-valence compounds, where M is a transition-metal element such as iron or manganese, L is a monodentate ligand such as pyridine, monosubstituted pyridine, or water, and S is a solvate molecule that is not explicitly coordinated to the central metal ions but stoichiometrically amalgamated in the crystal lattice. In what follows, each compound will be abbreviated as **[M, L, S]**. Figure 1 illustrates the molecular structure, with M ◘ iron and L ◘ pyridine, in the valence-detrapped state.

Intramolecular electron-transfer between the metal centers in a mixed-valence complex is usually treated by a theory incorporating vibronic interactions, such as the PKS theory (refs 6,7). The "extra" electron residing on the low-oxidation metal center is coupled with molecular vibrations *via* the vibronic interaction. In effect, the vibronic interaction induces a pseudo Jahn-Teller distortion of the molecule (ref. 8), in which the extra electron is localized on one particular metal center. In the case of an isolated mixed-valence molecule, the extra electron itinerates among the metal centers in the complex as a result of large-amplitude molecular vibration. This situation can be understood from the theoretical treatment by Kambara *et al.* (ref. 9). For one of the electronic states of the oxo-centered trinuclear mixed-valence molecule, the extra *d*-electron localizes on one metal ion, that is, the valency of the three metal ions is M(II)M(III)M(III). The distance between the M(II) ion and the central oxygen ion is at this point different from that between either M(III) and the central oxygen ion. The triangle whose apexes are three metal ions is distorted from an equilateral triangle. For the second electronic state, the extra *d*-electron itinerates on the three metal ions, that is, the electronic structure is delocalized. Since the three metal ions are equivalent to each other in this second electronic state, the M_3O triangle is equilateral. The adiabatic potential energy of the i-th electronic state E_i is a function of the nuclear displacement q and the direction of distortion θ. The dependence of the energies $E_i(q, \theta)$ on the magnitudes of q and θ is qualitatively changed depending on the magnitude of a characteristic parameter $\Delta (= \kappa\omega/\lambda^2)$, where κ is the force constant for the distortion mode, ω denotes the electron-transfer integral between two metal ions, and λ stands for the coupling constant of *d*-electrons with the distortion. As reproduced in Figs. 2a-2c (ref. 9), the adiabatic potential energies $E_i(q, \theta)$ along the direction θ_0 of a M-O bond can be classified into three types according to the magnitude of Δ. For the first type, the ground adiabatic potential surface provides three minima. In addition to these three potential minima, the second type gives the fourth minimum at $q = 0$, indicating a coherent electron-distribution over the three metal ions to form an equilateral triangle. Contrary to these two types, the third type brings about only a single minimum at q ◘ 0. Adiabatic potential energy surfaces for the ground electronic state of a mixed-valence M_3O complex calculated for two Δ ◘ 0.05 and 0.74 are drawn three-dimensionally in Figs. 2d and 2e (ref. 10).

When the mixed-valence complexes are aggregated in a crystal, the rate of intramolecular electron-transfer is seriously affected by environmental effects in the solid-state lattice.

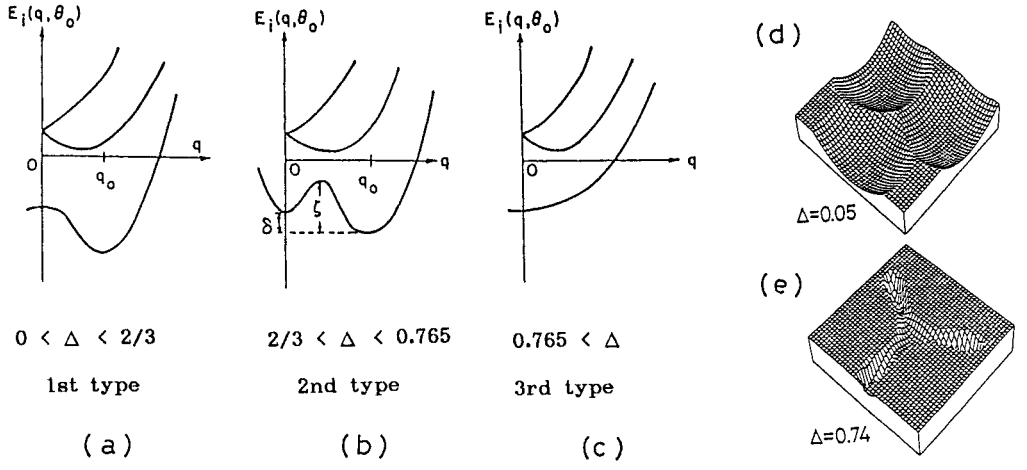

Fig. 2. (a)-(c): Three types of the adiabatic potential-energy surface for different values of Δ along the direction of an Fe-O bond (ref. 9). (d),(e): Three-dimensional drawing of the adiabatic potential-energy surface of the ground electronic state (ref. 10).

If the packing of molecules is very tight in the crystal, intramolecular electron-transfer is difficult. On the other hand, when large-amplitude intramolecular vibrations are appreciable, a cooperative crossover phenomenon between the valence-trapped and the valence-detrapped states is expected to occur. In fact, a series of these complexes exhibit interesting phase transitions (refs 4,5,10-20). These phase transitions have the character of an order-disorder transition involving the distortion dipoles that arise from the pseudo Jahn-Teller distortion in each complex.

The entropy gain due to the valence-detrapping phenomenon is straightforwardly related to the change in the number of microscopic states thermally accessible for the M_3O complex. Molecular configurations in the crystal are determined by the force field acting on each atom. The force field mainly consists of two contributions: one arises from the valence electrons, *i.e.* the adiabatic potential, and the other comes from neighboring molecules, *i.e.* the environmental effects. This effective force field can be designated as the mean-field potential. The number of microscopic states corresponds to the number of accessible (by tunneling or thermal activation) minima on the mean-field potential surface of the complex. At low temperatures, the M_3O complex is valence-trapped and has statically one of the isosceles triangular configurations. However, depending on the magnitude of Δ, the dynamically interconverting M_3O complexes in the high-temperature phase will either gain access to ***three*** microscopic states as shown in Fig. 2d, or to ***four*** microscopic states (Fig. 2e). In the former case, valence-detrapping gives an entropy gain of R ln 3 (= 9.13 $JK^{-1}mol^{-1}$), whereas in the latter case the entropy gain is R ln 4 (= 11.53 JK^{-1} mol^{-1}), where R is the gas constant.

Phase transitions in trinuclear complexes with R32 symmetry

When the ligand L is pyridine or 4-methylpyridine (4-Me-py), the complexes crystallize in a rather high-symmetry crystal system (rhombohedral: space group R 32) in their valence-detrapped phases and the solvate molecules sit on the C_3 axis (refs 13-16). In this section, we shall describe phase transitions encountered in these complexes. Heat-capacity measurements were made with an adiabatic calorimeter (ref. 21) and evaluated in terms of C_p, the molar heat capacity under constant pressure. The amount of sample used for measurements was ~15 g. As shown in Fig. 3, the **[Fe, py, py]** complex exhibits two kinds of phase transitions: one is a first-order phase transition at about T = 112 K and the other is a higher-order phase transition around T = 190 K (refs 5,12). Variable-temperature ^{57}Fe Mössbauer spectra (refs 4,14) show dramatic changes with temperature, as shown in Fig. 4. At temperatures below ~100 K, two quadropole-split doublets are seen: one characteristic of high-spin Fe(II) and the other of high-spin Fe(III). As the temperature is increased, an extra doublet appears abruptly around 110 K at the expense of the initial two doublets. This means that the new doublet arises from the electron-delocalized state. The spectrum eventually becomes a single doublet above ~190 K, indicating that the rate of intramolecular electron-transfer exceeds the ~10^7-10^8 s^{-1} rate which the Mössbauer technique can sense. It is of great interest that the low-temperature (LT) phase transition takes place at the temperature where the first Mössbauer spectrum change occurs and that the peak temperature of the high-temperature (HT) phase transition is identical with the temperature at which the Mössbauer spectrum becomes a single average doublet. Moreover, the large temperature range involved in the HT-phase transition fully overlaps the temperature region where the drastic spectrum change is occurring.

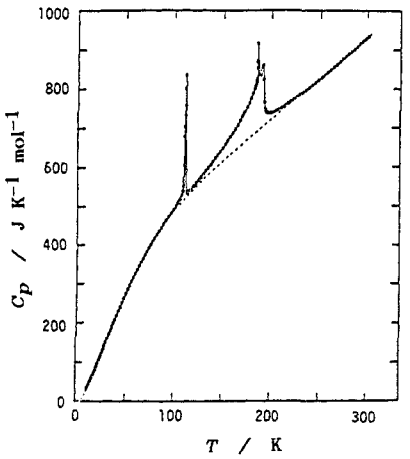

Fig. 3. Molar heat capacity of [Fe, py, py] (ref. 12).

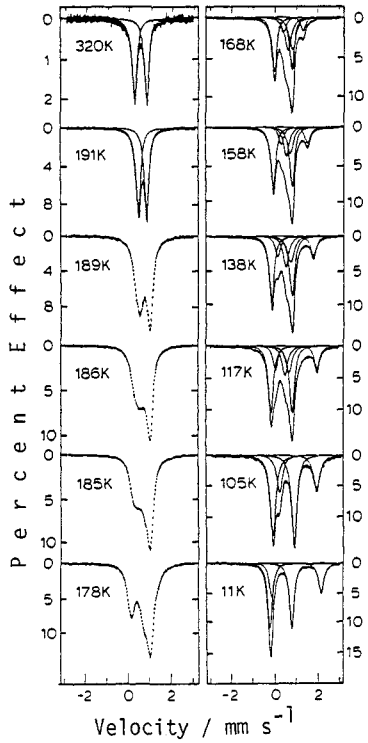

Fig. 4. Variable-temperature ^{57}Fe Mössbauer spectra for [Fe, py, py] (ref. 14). →

To estimate the excess thermodynamic quantities associated with the phase transitions, a "normal" heat-capacity curve was determined by an effective frequency-distribution method (ref. 22). The broken curve in Fig. 3 represents the normal heat capacity thus obtained. As shown in Fig. 5, the transition entropy ΔS for **[Fe, py, py]** approaches a value of $\sim R$ ln 2 at the LT-phase transition. With a further increase in sample temperature, ΔS gradually increases to become (30.58±0.83) JK^{-1}mol^{-1} at temperatures far above the HT-phase transition. Since the entropy gain due to valence-detrapping is either R ln 3 or R ln 4, the observed transition entropy ($\sim R$ ln 39.6) obviously contains extra contributions other than the intramolecular electron-transfer. A clue to the extra candidates lies behind its crystal structure. A drawing of the molecular packing in the valence-detrapped HT-phase is shown in Fig. 6 (ref. 14). Along the C_3 axis, Fe_3O complexes and solvate molecules occupy alternating sites of 32 symmetry. That is, each pyridine solvate molecule is sandwiched between two Fe_3O complexes. The plane of the pyridine solvate molecule is perpendicular to the Fe_3O plane. As required by the presence of the C_3 axes along which the Fe_3O complexes are stacked, the pyridine solvate molecules are disordered (at least three orientational positions). Solid-state ^{2}H NMR data on the deuterated pyridine sample also showed that the pyridine solvate molecule converts from being static to dynamically interconverting between ***twelve*** different orientations (ref. 14). The plane of the pyridine molecule jumps between three positions about the crystallographic C_3 axis. In each planar position, the pyridine solvate molecule librates between four positions, each with two carbon atoms on the C_3 axis (Fig. 7a). If each Fe_3O complex converts from being statically distorted in one state to interconverting dynamically between ***three*** vibronic states when the complex is heated from low temperatures, this contributes R ln 3 to the entropy gain. The sum of R ln 3 for the Fe_3O constituents and R ln 12 for the solvate molecules gives ΔS = 29.79 JK^{-1}mol^{-1}. This value agrees well with the observed ΔS ◻ (30.58±0.83) JK^{-1} mol^{-1}. This fact provides conclusive evidence that the intramolecular electron-transfer *does* proceed in cooperation with orientational disordering of the solvate molecules. In fact, although the pyridine solvate molecule in permanently distorted nonmixed-valence complex $[Fe(III)_2Co(II)O(O_2CCH_3)_6(py)_3](py)$ undergoes free ring-rotation about its pseudo C_6 axis even at low temperatures and the plane of the pyridine molecule jumps between three positions about the crystallographic C_3 axis at high temperatures (Fig. 7b), this complex does not exhibit a phase transition but a broad heat-capacity hump centered around 150 K (ref. 20). The observed entropy gain (10.3 JK^{-1}mol^{-1}) accords well with the expected value, R ln 3 (= 9.13 JK^{-1}mol^{-1}).

For the mixed-valence complex **[Mn, py, py]**, in which only the central iron ions of **[Fe, py, py]** are substituted for manganese ions, its transition behavior is drastically altered (ref. 15). As shown in Fig. 8a, this complex brings about a sharp first-order phase transition at 184.7 K and the transition entropy (Fig. 5) amounts to 35.77 JK^{-1}mol^{-1} (ref. 10). Variable-temperature ^{2}H NMR data of the deuterated pyridine complex (ref. 18) revealed that each pyridine solvate molecule is rapidly reorienting about its local pseudo C_6 axis and, moreover, the pyridine plane jumps between three positions about the crystallographic C_3 axis, in each

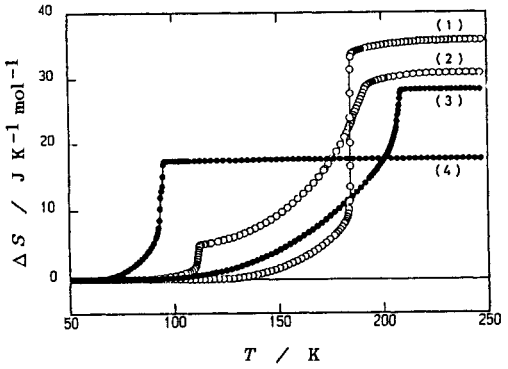

Fig. 5. Acquisition of the transition entropy of (1) **[Mn, py, py]**, (2) **[Fe, py, py]**, (3) **[Fe, py, $CHCl_3$]** and (4) **[Fe, 4-Me-py, $CHCl_3$]**.

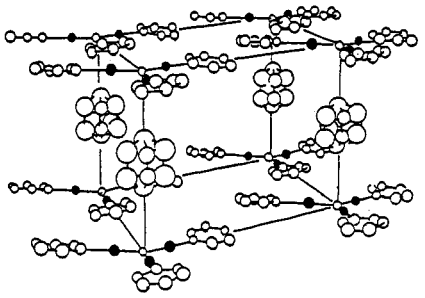

Fig. 6. Crystal structure of **[Fe, py, py]** (ref.14). The acetato ligands are not shown. Crystallographic C_3 axis runs through the central oxygen atoms of Fe_3O complexes.

of which the pyridine plane is tilted from the C_3 axis by $\sim 15°$ (Fig. 7c). In this case, the expected entropy gain due to the solvate molecule would be R ln 18. If one assumes that **four** minima in the mean-field potential surface are established in the valence-detrapped HT-phase, its entropy gain is R ln 4. The sum of these two contributions (35.56 $JK^{-1}mol^{-1}$) agrees with the observed value 35.77 $JK^{-1}mol^{-1}$.

As in the case of **[Mn, py, py]**, the mixed-valence complexes **[Fe, py, $CHCl_3$]** and **[Fe, 4-Me-py, $CHCl_3$]** showed a single-step first-order phase transition. As shown in Fig. 8b, **[Fe, py, $CHCl_3$]** exhibited a phase transition at 208 K with ΔS □ (28.10±0.44) $JK^{-1}mol^{-1}$ (ref. 17), while **[Fe, 4-Me-py, $CHCl_3$]** showed a phase transition at 94 K with ΔS = (17.18 ±1.42) $JK^{-1}mol^{-1}$ (ref. 19) (see Fig. 5). These transition temperatures just correspond to those at which the third quadropole-split doublet arising from the electron-delocalized state appears in their ^{57}Fe Mössbauer spectra (ref. 16). Variable-temperature ^2H NMR of the deuterated chloroform complexes (refs 16,19) revealed that the $CHCl_3$ solvate molecules in **[Fe, py, $CHCl_3$]** cooperatively convert from being static in one lattice position to jumping between **eight** positions in the phase transition, whereas the $CHCl_3$ molecules in **[Fe, 4-Me-py, $CHCl_3$]** only start jumping between **two** positions where the C-H vector is either pointing up or down along the C_3 axis (Figs. 7d and 7e). The valence-detrapping phase transition in both cases involves each Fe_3O complex converting from being statically trapped in one vibronic state to dynamically interconverting between **four** vibronic states. For both complexes this contributes $\Delta S = R$ ln 4. As compared in Table 1, the observed transition entropies for these two complexes also agreed with the calculated values.

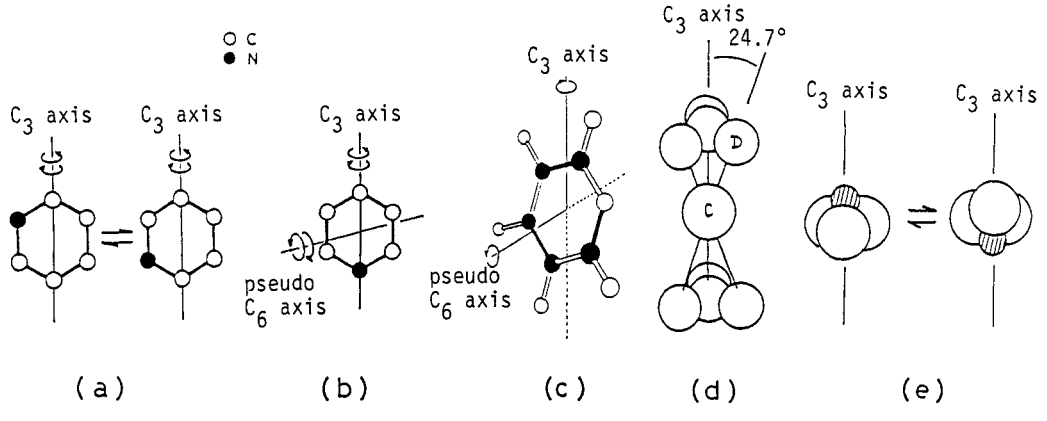

Fig. 7. Orientational disordering of the solvate molecules in the crystal lattice. (a) Pyridine in **[Fe, py, py]** (ref. 14), (b) pyridine in $[Fe(III)_2Co(II)O(O_2CCH_3)_6(py)_3](py)$ (ref. 20), (c) pyridine in **[Mn, py, py]** (ref. 18), (d) deuterated chloroform in **[Fe, py, $CHCl_3$]** (ref. 16) and (e) chloroform in **[Fe, 4-Me-py, $CHCl_3$]** (ref. 19).

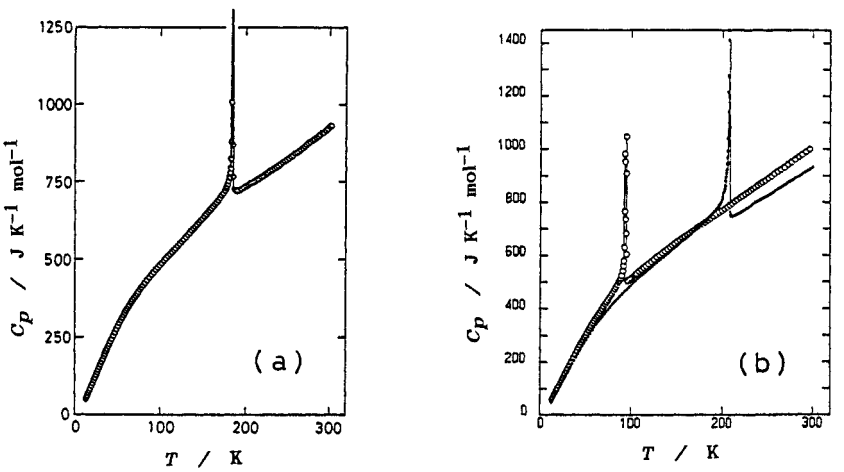

Fig. 8. Molar heat capacities of (a) **[Mn, py, py]** (ref. 10), and (b) **[Fe, py, $CHCl_3$]** (●) (ref. 17) and **[Fe, 4-Me-py, $CHCl_3$]** (○) (ref. 19).

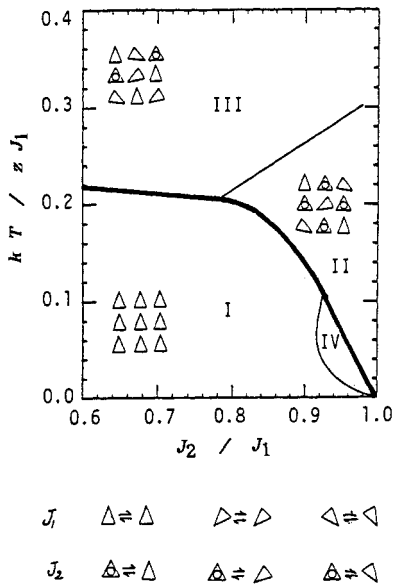

Fig.9. The phase diagram obtained by Stratt and Adachi (ref. 23). Thick curve corresponds to a first-order while thin curves are of second-order transitions.

A simple but fundamental question arises here as to why only the **[Fe, py, py]** complex exhibits two phase transitions (a first-order phase transition at low temperatures and a higher-order one at high temperatures) in comparison to a single first-order phase transition in other complexes with *R* 32 symmetry. Stratt and Adachi (ref. 23) took an imaginative and insightful approach to developing a theoretical model for the phase transitions in the mixed-valence Fe_3O complexes, although the effect of solvate molecule dynamics was ignored. Their phase diagram is shown in Fig.9. When the ratio (J_2/J_1) of two interaction energies J_2 and J_1 is less than ~0.78, their model brings about a single first-order phase transition, while for an appropriate range ($0.78 < J_2/J_1 < 0.92$) double phase transitions are possible: one is of a first-order and the other is of a second-order.

Phase transitions in the trinuclear complexes with lower symmetry than R32

When the pyridine ligand molecule is replaced by a *meta*-substituted pyridine (3-methylpyridine), the resultant symmetry of the mixed-valence complex $[Fe(III)_2Fe(II)O(O_2CCH_3)_6(3\text{-Me-py})_3]S$ is considerably lowered. Compounds having either S = 3-Me-py or S = toluene crystallize in

TABLE 1. Entropy gain at the phase transitions observed in the mixed-valence complexes with the formula $[M(III)_2M'(II)O(O_2CCH_3)_6L_3]S$ (in the unit of $JK^{-1}mol^{-1}$).

Complex				T_C/K	Entropies			
M	M'	L	S		ΔS(M)*1	ΔS(S)*2	ΔS(calcd)*3	ΔS(obsd)
Fe	Fe	py	py	112, 191	*R* ln 3	*R* ln 12	29.79	30.58±0.83
Fe	Co	py	py	150	---	*R* ln 3	9.13	10.3
Mn	Mn	py	py	185	*R* ln 4	*R* ln 18	35.56	35.77
Fe	Fe	py	$CHCl_3$	208	*R* ln 4	*R* ln 8	28.82	28.10±0.44
Fe	Fe	4-Me-py	$CHCl_3$	94	*R* ln 4	*R* ln 2	17.29	17.18±1.42
Fe	Fe	3-Me-py	3-Me-py	181, 282	*R* ln 3	*R* ln 2	14.90	13.71±0.65
Fe	Fe	3-Me-py	toluene	293	*R* ln 3	*R* ln 2	14.90	15.07

*1: Entropy gain due to the M_3O complex, *2: entropy gain due to the solvate molecule S, *3: ΔS(calcd) ≡ ΔS(M) + ΔS(S).

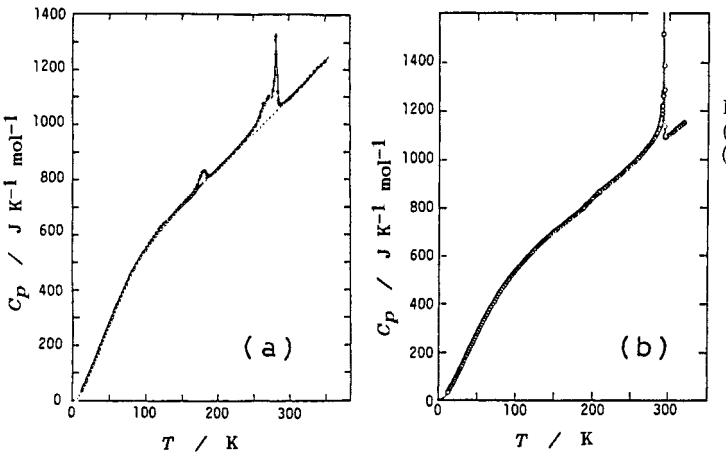

Fig. 10. Molar heat capacities of (a) **[Fe, 3-Me-py, 3-Me-py]** (ref. 25) (b) **[Fe, 3-Me-py, toluene]** (ref. 26).

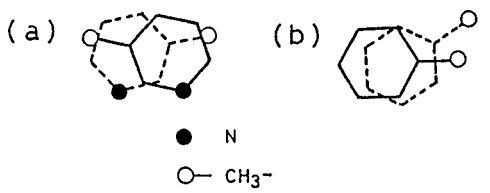

Fig. 11. Orientational disordering of (a) the 3-methylpyridine solvate molecule in **[Fe, 3-Me-py, 3-Me-py]** and (b) toluene in **[Fe, 3-Me-py, toluene]** (ref. 24).

the triclinic space group $P\bar{1}$ (ref. 24). Their ^{57}Fe Mössbauer spectra (ref. 24) show two quadropole-split doublets in the area ratio of two (high-spin Fe(III)) to one (high-spin Fe(II)) at temperatures below ~100 K. Increasing the sample temperature above ~100 K leads to the appearance of a third average-valence doublet with a small spectral area. Eventually the spectrum changes to become a single-average doublet at high temperatures. In contrast to the complexes with *R* 32 symmetry, however, X-ray structural work carried out at 298 K (ref. 24) has revealed that the Fe_3O triangles of these complexes are not exactly equilateral. Moreover, the solid-state packing arrangement consists of Fe_3O units arranged two-dimensionally in layers with the solvate molecule located in an open space made by three neighboring Fe_3O molecules. These Fe_3O complexes adopt a conformation with all three 3-methylpyridine ligands approximately perpendicular to the Fe_3O plane.

One may ask how these low-symmetry complexes manifest phase transitions in comparison to those of the *R* 32 complexes. Figures 10a and 10b represent molar heat capacities of **[Fe, 3-Me-py, 3-Me-py]** (ref. 25) and **[Fe, 3-Me-py, toluene]** (ref. 26), respectively. As listed in Table 1, their transition entropies are (13.17±0.65) and 15.07 $JK^{-1}mol^{-1}$, respectively. Since the Fe_3O triangles in these complexes cannot take equilateral form in the valence-detrapped HT-phase, the entropy gain arising from the intramolecular electron-transfer would be expected to be *R* ln 3 (= 9.13 $JK^{-1}mol^{-1}$) at most. Therefore, the remaining entropy gains are attributable to the onset of molecular motions of the solvate molecules at the phase transition. A single crystal ^{2}H NMR study of the deuterated complexes (ref. 24) shows that at room temperature the 3-methylpyridine and toluene solvate molecules are jumping between **two** lattice positions as shown in Fig. 11. Consequently, the expected entropy gain due to the solvate molecule is *R* ln 2 for both the complexes. As can be seen from Table 1, the sum of these two contributions (14.90 $JK^{-1}mol^{-1}$) accounts for the observed values very well.

CONCLUDING REMARKS

Intramolecular electron-transfer events in the mixed-valence iron complexes were initially studied by ^{57}Fe Mössbauer spectroscopy. Dramatic change in the spectrum was the conversion from a valence-trapped state at low temperatures to a valence-detrapped state at high temperatures on the time scale of ^{57}Fe Mössbauer spectroscopy (~10^7-10^8 s^{-1}). At this stage, however, one could not conclude whether the interconversion rate would be altered abruptly or gradually with a change in temperature. For the former case, one can expect phase transition phenomena but for the latter case no phase transition or a very sluggish one. Since calorimetry belongs to an experimental method characterized by the slowest time-scale, it serves as a powerful tool to see whether a phase transition exists or not. Our calorimetric studies clearly revealed that the intramolecular electron-transfer in the solid state *does* proceed *via* phase transition(s). Moreover, the entropy gains at the phase transitions provided conclusive evidence of the interplay of the intramolecular electron-transfer and the orientational disordering of the solvate molecules in the lattice. The solvate molecules assist the intramolecular electron-transfer not only as a spacer in the lattice making room for

the large-amplitude motion of a mixed-valence complex, but also as an interaction path between the mixed-valence complexes. Interaction between the distortion dipole of a mixed-valence complex and the permanent dipole of a given solvate molecule seems to be responsible for the mechanism of phase transitions. Needless to say, one cannot elucidate what has happened at a microscopic level solely from calorimetric studies. In the present paper, all the conclusions have been based not only on calorimetric results, but also those derived from various spectroscopic and structural studies. The importance of the complementary nature of macroscopic and microscopic aspects should be again emphasized.

Acknowledgements The authors would like to thank Professor H. Sano of Tokyo Metropolitan University and Professor T. Kambara of the University of Electro-Communications for valuable discussion, and K. Kaji, Y. Shiomi, Dr. Y. Nagano, Dr. M. Nakano, A. Nishimori and Miss Y. Kaneko for their collaboration in heat-capacity measurements.

REFERENCES

1. P. Day, *Int. Rev. Phys. Chem.* **1**, 149-193 (1981).
2. *Mixed-Valence Compounds: Theory and Applications in Chemistry, Physics, Geology, and Biology*, edited by D. B. Brown, Reidel, London (1980).
3. C. Creutz, *Prog. Inorg. Chem.* **30**, 1-73 (1983).
4. S. M. Oh, D. N. Hendrickson, K. L. Hassett and R. E. Davis, *J. Am. Chem. Soc.* **106**, 7984-7985 (1984).
5. S. M. Oh, T. Kambara, D. N. Hendrickson, M. Sorai, K. Kaji, S. E. Woehler and R. J. Wittebort, *J. Am. Chem. Soc.* **107**, 5540-5541 (1985).
6. S. B. Piepho, E. R. Krausz and P. N. Schatz, *J. Am. Chem. Soc.* **100**, 2996-3005 (1978).
7. K. Y. Wong and P. N. Schatz, *Prog. Inorg. Chem.* **28**, 369-449 (1981).
8. I. B. Bersuker, *The Jahn-Teller Effect and Vibronic Interactions in Modern Chemistry*, Plenum Press, New York (1984).
9. T. Kambara, D. N. Hendrickson, M. Sorai and S. M. Oh, *J. Chem. Phys.* **85**, 2895-2909 (1986).
10. M. Nakano, M. Sorai, J. B. Vincent, G. Christou, H. G. Jang and D. N. Hendrickson, *Inorg. Chem.* **28**, 4608-4614 (1989).
11. S. M. Oh, D. N. Hendrickson, K. L. Hassett and R. E. Davis, *J. Am. Chem. Soc.* **107**, 8009-8018 (1985).
12. M. Sorai, K. Kaji, D. N. Hendrickson and S. M. Oh, *J. Am. Chem. Soc.* **108**, 702-708 (1986).
13. S. E. Woehler, R. J. Wittebort, S. M. Oh, D. N. Hendrickson, D. Inniss and C. E. Strouse, *J. Am. Chem. Soc.* **108**, 2938-2946 (1986).
14. S. E. Woehler, R. J. Wittebort, S. M. Oh, T. Kambara, D. N. Hendrickson, D. Inniss and C. E. Strouse, *J. Am. Chem. Soc.* **109**, 1063-1072 (1987).
15. J. B. Vincent, H. R. Chang, K. Folting, J. C. Huffman, G. Christou and D. N. Hendrickson, *J. Am. Chem. Soc.* **109**, 5703-5711 (1987).
16. H. G. Jang, S. J. Geib, Y. Kaneko, M. Nakano, M. Sorai, A. L. Rheingold, B. Montez and D. N. Hendrickson, *J. Am. Chem. Soc.* **111**, 173-186 (1989).
17. Y. Kaneko, M. Nakano, M. Sorai, H. G. Jang and D. N. Hendrickson, *Inorg. Chem.* **28**, 1067-1073 (1989).
18. H. G. Jang, J. B. Vincent, M. Nakano, J. C. Huffman, G. Christou, M. Sorai, R. J. Wittebort and D. N. Hendrickson, *J. Am. Chem. Soc.* **111**, 7778-7784 (1989).
19. H. G. Jang, R. J. Wittebort, M. Sorai, Y. Kaneko, M. Nakano and D. N. Hendrickson, *J. Am. Chem. Soc.* **112**, in press (1990).
20. H. G. Jang, K. Kaji, M. Sorai, R. J. Wittebort, S. J. Geib, A. L. Rheingold and D. N. Hendrickson, *Inorg. Chem.* **30**, in press (1990).
21. M. Sorai, K. Kaji and Y. Kaneko, *J. Chem. Thermodyn.* (in press).
22. M. Sorai and S. Seki, *J. Phys. Soc. Jpn.* **32**, 382-393 (1972).
23. R. M. Stratt and S. H. Adachi, *J. Chem. Phys.* **86**, 7156-7163 (1987).
24. S. M. Oh, S. R. Wilson, D. N. Hendrickson, S. E. Woehler, R. J. Wittebort, D. Inniss and C. E. Strouse, *J. Am. Chem. Soc.* **109**, 1073-1090 (1987).
25. M. Sorai, Y. Shiomi, D. N. Hendrickson, S. M. Oh and T. Kambara, *Inorg. Chem.* **26**, 223-230 (1987).
26. A. Nishimori, Y. Nagano, M. Sorai and D. N. Hendrickson (unpublished).